Original Article

Analysis of erosion rill development under rainfall events using structure-from-motion photogrammetry – a case study from Kielce (Holy Cross Mts., Poland)

Piotr Tomasz KOPYŚĆ https://orcid.org/0000-0001-5503-0838; e-mail: piotr.kopysc@phd.ujk.edu.pl

Jan Kochanowski University, Institute of Geography and Environmental Sciences, Uniwersytecka 7, 25-406 Kielce, Poland

Abstract: The development of erosive landforms such as rills, ditches, slits, and gullies depends on many environmental factors; thus, the rate of the development of each individual form differs. In this paper, the author presents a case study of two erosion rills located on a hiking trails (Holy Cross Mts.) resulting after 2 years of monitoring in which the process of their evolution was precisely analyzed. Once established, such landforms develop over time with variable rates and can represent multiple different stages. Moreover, the final result of the rill development hardly reminds their original form and does not allow for interpretation of the events that affected it in the recent past. Therefore, the main objective was to determine the volumetric changes of erosion rills created by the surface runoff on both sections, during two years of observation. Additional objectives included a description of the physical and meteorological parameters, important in the development process and a comparison of them to the volumetric changes of each period. Using the Structure-from-motion (SfM) photogrammetry technique, monitoring procedures have been performed quickly offering sufficient accuracy. For direct comparison, the digital elevation model of difference (DoD) method was used, enabling the calculation of volume. The results showed that the erosion to deposition ratio was more disproportionate during storm events or periods with higher depth of rainfall. Total erosion to deposition balance for the entire monitoring period was negative and equal to 1448.84 kg or 410 Mg/ha for the first erosion rill and 1059.5 kg or 300 Mg/ha for the second rill. Both erosion rills developed differently. The first erosion rill developed by linear cut into deeper and wider form, while the other, steeper rill, evolved from plunge pools merging together into deeper and wider form.

Keywords: Erosion; SfM; DoD; Rainfall; Microtopography

1 Introduction

Hiking trails that lead through unpaved forested paths and roads are known to be subject to degradation (Cole 1991; Wimpey and Marion 2010; Tomczyk et al. 2016; Meadema et al. 2020; Sahani and Ghosh 2021) due to natural and anthropogenic processes which have been studied by numerous authors (Ballantyne and Pickering 2015; Salesa and Cerdà 2020). Therefore, they are prone to the formation of erosion forms such as rills, which are responsible for further land degradation. Because of the existence of active rills on the trails surfaces, there are increasing sedimentation, widening of the road, disruptions to pavement morphometry, accelerated surface runoff, and vegetation loss. Soil erosion is one of the most crucial issues affecting hiking trails and

areas of their extent. Linear erosion processes are responsible for the creation and destruction of rills, interrills, ditches, and smaller and larger gullies that evolve over time into their larger variants. Rainfall events and surface runoff caused by them have been identified as the main causes of the rill development (Starkel 2011). Within recent times their intensity grows in the temperate zone (Trenberth 2011). Factors such as "heat island" connected to human activity in the cities also do affect the frequency of extreme rainfall events (Ciupa 2009; Ciupa and Suligowski 2020; Michalczyk et al. 2012; Wałek 2019). Therefore, it is important to know the rill development rates, especially knowing their potential to transform into permanent gullies (Martnez-Casasnovas et al. 2002).

The ongoing erosion of such landforms increases their size which leads to higher repair costs with each stage of their development. This issue is especially important on mentioned hiking trails which are a part of the tourist infrastructure exposed to rill erosion, which is amplified by rainfall events. Such repairs are often a necessity in mountainous areas where fixing and reorganizing the trails has become a common practice as a form of environmental protection (Tomczyk and Ewertowski 2013; Tomczyk et al. 2016; Fidelus-Orzechowska et al. 2021). In the past, a great amount of work has been done by the scientific community to study rill erosion caused by rainfall events in order to avoid the consequences of such rills development. It was done in multiple controlled laboratory experiments (Chaplot et al. 2011; Fang et al. 2014; Shen et al. 2015; He et al. 2017; Yang et al. 2021; Sadeghian et al. 2021) as well as with measurement and observation performed in the field (Martnez-Casasnovas et al. 2002; Arnáez et al. 2004; Bouchnak et al. 2009; Comino et al. 2015; Zhang et al. 2019; Cao et al. 2021; Wang et al. 2021). In those studies, the rate of erosive forms development has been recorded. With each new result, scientists have established the groundwork for a better understanding of the linear erosion phenomenon, thus opening new possibilities among which are machine learning modeling in erosion susceptibility mapping (Wang et al. 2021; Nourani et al. 2022) as well as forecasting other important environmental factors (Chen et al. 2022). In their work, an emphasis was placed on the role of terrain characteristics, such as slope and landform gradient (Berger et al. 2010), position (Beullens et al. 2014), geometric properties

such as length and width (Govers et al. 2007; Comino et al. 2015), rainfall intensity (Shen et al. 2015; Shen et al. 2018, 2019), splash erosion (Angulo-Martinez et al. 2012), soil properties (Kiani-Harchegani et al. 2018), land use (Yang and Liang 2004; Wang et al. 2021) and vegetation cover (Woo et al. 1997). However, simplifications and assumptions under laboratory conditions can affect the results, causing erosion rates to be underestimated or overestimated. Furthermore, field studies are often difficult to perform, as a vast number of factors impact the outcome (Eagleston and Marion 2020; Ou et al. 2021). Therefore, for a wider understanding of the rill erosion development, studies need to be conducted in many areas. Such field observation studies in regards to the unpaved roads were not conducted in the western Holy Cross Mountains as of yet. A popular method of recording erosion in the field is the use of systems and devices to catch eroded soil particles. However, installation of such devices would have eliminated the recreational movement from the trail. Therefore, a non-invasive method must be applied such as measurements of morphometric characteristics over time, in order to not limit a recreational movement over the trail.

Recently, with the popularization of unmanned aircraft vehicles (UAV) and high-resolution photography, such measurements can be performed with the use of LiDAR data or photogrammetry (Zhang et al. 2019; Salesa et al. 2020). Structure-from-motion (SfM) is one such photogrammetry technique that allows for capturing 3D structures from 2D pictures. This technique was further described in other studies (Vinci et al. 2017; Salesa et al. 2020; Kopyść 2020). SfM has been used successfully in several studies using unmanned aerial vehicles (Xu et al. 2020) and terrestrial equipment (Yang et al. 2021).

In this work, the author examined the development of two erosion rills located on forested roads and the changes that occurred over time within 2 year period with the inclusion of rainfall events. The main goal of this study was to estimate the erosion rates during different seasons, by the structure-from-motion (SfM) technique. An emphasis was put on this objective in order to calculate the rate of the development of such forms in the future. Obtained rates of development were also compared to the characteristics of each rill together with the physical properties and meteorological conditions of each

monitored period.

2 Study Area

The two monitored rills are located in the

Posłowickie mountain range in southern part of Kielce city. First of them is located on the northeastern slope of Pierścienica Mountain (50°83'87"N, 20°60'01"E), while the second is on the eastern slope of Biesak Mountain (50°83'47"N, 20°57'70"E). This mountain range is part of the Holy Cross Mountains located
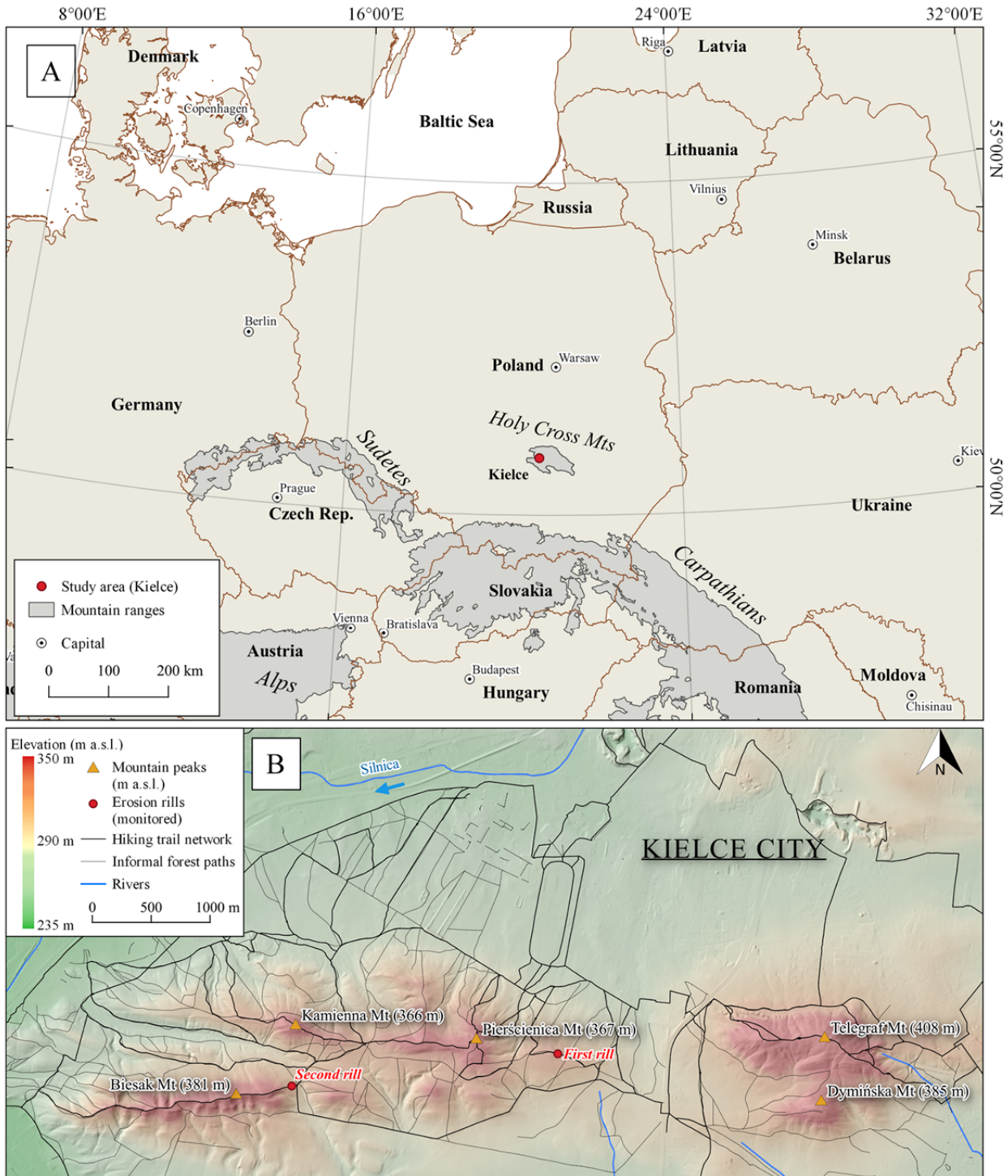

Fig. 1 Map of the study area. A - Location of Kielce City and Holy Cross Mountains; B - Posłowickie mountain range in the southern part of Kielce city (Data: European Environmental Agency).

north of the Carpathian mountain range (Fig. 1).

The landscape of the Posłowickie and Dyminskie Mountain range where Pierścienica and Biesak Mountain is located is composed of longitudinal ridges and valleys. The main ridges are composed of sandstones originating from the early Cambrian period. During the Pleistocene epoch, the mountains were affected by the Riss glaciation. Due to the complexity of the geological structure and long history of events, the late Pleistocene and Holocene epoch soils formed diverse structures in the area. On the slopes of Biesak and Pierścienica, mountain soils are mostly sandy, with low clay and silt contents (Strzemski 1965; Filonowicz 1973). Lithological properties have been confirmed by the author's investigation in the area. The soil on the trails lacks gravel or stones (>2 mm). Although both trails have similar sand distribution, the trail soils have had up to an 80% smaller share of silt and clay (< 0.1 mm) compared to the reference material from off the trail, which indicates that they are actively participating in surface runoff. Throughout the Posłowickie mountain range, a 62.5 km trail network has been created for the use of tourists and recreationists, with over 150 km of informal forests paths. Upon hiking trails, multiple erosive rills were spotted during the preliminary field investigation, which later on was monitored during main studies. First of the erosion rills that were monitored, is located directly on the

hiking trail surface, mainly used for biking and pedestrian use, however, singular tracks of motorcycles and horse tracks have been recorded during the monitoring. Although the entire mountain area is covered by forest, the trail has been partially exposed by tree felling in the last 5 years. The use of the trail throughout the years has exposed and highly compacted the soil layer. The second rill, now located at the side of the hiking trail, originally developed in its axis prior to 2016. This hiking trail has a similar level of use to the one where the first rill is located, with pedestrians and bikers commonly spotted during observation, while horses and vehicles tracks were absent. In the area of the first rill, vegetation densely covers both sides of the trail, therefore limiting the ability to bypass obstacles. At the same time, the second rill, has fewer plants on its sides, while crowns of coniferous trees cover the surface from the direct rainfall. Lack of small vegetation caused the creation of the new road where older rill is now omitted by the hikers (Fig. 2). The age of the first rill has been estimated on the 24 points per m² aerial LiDAR data, which shows a very recent development as its structure is absent in data from 2019. The second rill has been spotted on the same LiDAR data as well as prior data from 2016 but absents in data from 2011. One of the main differences between both rills is a road gradient and rill axis to slope direction alignment angle (Table 1). The second rill has much

Fig. 2 First and second rill during SfM scanning, Marker P2 as an example of one of the eight GCPs placed on each test plot, arrow points to painted target.

Table 1 Characteristics of each monitored rill

Rill characteristics	Rill 1	Rill 2
Location of the rill	50°83'78" N, 20°60'89" E	50°83'44" N, 20°57'70" E
Altitude above sea level (m)	335	380
Area of the measurements (m²)	26.89	43.86
Age of the rill (years)	< 2	5 - 8
Slope (°)	8.0	15.6
Rill axis to slope direction angle (°)	37.00	2.53
Road segment length (m)	60	270
Road width (m)	2.40	5.10
Soil density (g/cm³)	1.831	1.612
Runoff contribution area (m²)	539	3125
Number of SfM scans	8	7

more favorable conditions to develop its size than the first one with a larger road gradient and near 0-degree rill to slope direction alignment angle.

In the study area, the most intense rainfall events occur during the summer season. The annual rain depth ranges from 580 to 720 mm for the Holy Cross Mountains. In 2020, the total rainfall for the study area was equal to 592.6 mm, while for 2021 it has been 693 mm. In 2020 the month with the highest rainfall depth was June (151.1 mm) while in 2021 it was August (194.8 mm). Months with the least rain were March and November in both years with rainfall depth value below 20 mm for each month. During the rills monitoring, the number of days with a sum of rainfall depth above 5mm for the first rill was equal to 71 while for the second it was 67. Out of those days, those on which intensity was above 90th percentile of all the rainfall events during monitoring (>2.7 mm/h) and length longer than 0.5 hours were the most intensive. The first rill was exposed to 19 high-intensity rainfall events from March 2020 to November 2021. The second rill received 20 of such events in the same period. The average length of those events was equal to 3.6 hours. Such events are not considered extreme since much more intensive rainstorms associated with the movement of cold weather fronts are possible in the study area (Suligowski 2014; Szeląg et al. 2020). The year 2020 was dryer than 2021 in Kielce as mean relative humidity was equal to 77.5% in 2020 and 79.4% for 2021, which was a result of a dry period during summer in 2020 where maximum temperatures reached 32 degrees Celsius on multiple days (IMWM data – Appendix 1).

Because the mountain range is located near the Kielce city border, it is easy to access, and therefore serves as a major recreational destination for tourists and Kielce residents alike, resulting in more constant use of the trail throughout the year, instead of seasonal use (Mityk 1993).

3 Methods

3.1 Field investigation

Before the monitoring started a larger-scale field investigation has taken place in the Posłowickie mountain range in order to find testing plots, with a potential to rill erosion. During that time a total of 12 km of hiking trail segments have been surveyed, chosen from a trail network, where road surface inspection took place every 20 meters. In the preliminary investigation, a total of 92 erosive rills has been counted with length from 2 to 18 meters out of which 20 have had their depth above 30 cm. Multiple erosive forms have been marked for monitoring out of which two erosion rills were monitored over time. Both locations have been designated on the following criteria: road gradient - above 5 degrees, type of the road - unpaved, road axis to slope direction alignment angle - below 40 degrees, mean terrain roughnesses of the trail - above 0.15. The final criteria were a potential of the surface to develop into a larger rill. In order to monitor rills changes over time, the SfM photogrammetry technique has been applied in the field. A total of 13 scans has been made of both rills, from March 2020 to November 2021. A usual interval of scanning was 3 months, however, after the intensive rainfall event took place, an additional scan was performed in order to capture its effects on both rills. When two 10 meter long, scanning test plots has been chosen for an investigation, a set of preparations took place on each of them. On both sides of the road, 4 ground control points (GCPs) have been established, with a total number of 8 for each testing plot. Those were spray-painted wooden plugs that were present in the field for the entire monitoring period. GCPs position has been obtained with the use of a GPS receiver (Trimble GeoXH 2008 series) and then corrected by a manual series of measurements of distances and azimuth to the nearest trees of each GCP with the use of a laser measuring tool (Bosch GLM 30). With 8 GCPs established on the testing plots, both plots have been divided into 3 rectangles, which were subject to a series of photographs from multiple angles. Pictures were taken with a smartphone camera

(Xiaomi 9T Pro) placed on a tripod, with the settings as follows: resolution - 48 Mpix, shutter speed 1/250, ISO 1600, lens set to wide, and focus of the camera set to manual with adjustments in the field. The usual distance from the camera lens to the erosion rill was approximately 1.5 meters. During the image acquisition, a set of markers (8 for each testing plot) has been placed in the location of the GCPs in the form of wooden stake (40 cm long) with painted "X" signs on them (L1-4 and P1-4) (Fig. 2). Markers also had an additional purpose as their height from the ground has been measured in order to estimate the vertical error of processed data. The photography sessions were performed for the first rill 8 times. In 2020 SfM sessions were performed on 27th April, 6th August (spring - summer 2020), 24th August (4 hours storm event), and 2nd November (summer - autumn 2020). In 2021 it was 18th April (winter 2021), 20th July (spring - summer 2021), 3rd September (18 hours storm event), and 29th October (summer - autumn 2021). The second rill was subject to SfM scanning 7 times. In 2020 it was 2nd May, 23rd July (spring - summer 2020), and 23rd October (summer - autumn 2020), while in 2021 it was on 9th April (winter 2021), 30th July (spring - summer 2021), 3rd September (18 hours storm event), and 31st of October (summer - autumn 2021). During the monitoring period, in spring 2021 two separate soil samples were collected to analyze their physical properties for each rill. One was collected directly from below the rill, and the other was reference material collected 3 meters from the sides of the trail. Samples were taken from the surface layer (A) under the organic layer (O). The soil samples were prepared for analyses by drying, removing organic matter, and grinding in a porcelain mortar. Samples were then placed on sieves and shaken for 10 minutes with an amplitude of 0.8 mm using Retsch AS 200 laboratory equipment.

3.2 Data processing

Every SfM field session resulted in 250 to 300 high-resolution pictures. In order to transform this data into 3D point clouds, they have been imported into an Agisoft Metashape Pro (ver. 1.6) software (Fig. 3). The first stage of the procedure was to estimate image quality by using one of the tools from mentioned software. Pictures with a quality value below 0.7 have been removed. Pictures above the quality threshold have had their contrast increased by 30% in order to

smooth the alignment process and detect details of the scanned rills. Dataset of pictures was then subject for "Align Photos" tool that searches for common points in pictures called "Tie Points". The setting of the Align Photos tool was as follows: quality – highest, key point limit – 60000 tie point limit – 6000, with adaptive camera model filtering option turned on. After tie points cloud has been obtained it has been filtered in order to remove points with low confidence levels. The following criteria with the use of gradual selection tool have been applied for the filtering: Tie point present on 3 pictures or more, reprojection error – bellow 1.0 pix, reconstruction uncertainty – below 40, projection accuracy bellow 10. All tie points that did not match these criteria have been removed and did not take part in dense point cloud creation. Tool "optimize camera alignment" has been used to optimize point locations and estimate tie point covariance. With it, final filtering of the tie point cloud has been applied, by removing points with covariance higher than 1 cm. After that, dense point cloud has been created with the settings as follows: quality – medium, depth filtering – aggressive, and option to calculate point colors and confidence set to "on". The final dense cloud has also been filtered with the criteria of point confidence below 10%. Dense point clouds from each SfM scan have been exported to the *.las* file and imported to CloudCompare (ver. 2.10) software. Before comparison was made each cloud has been resampled from 0.3 cm resolution to 1 cm resolution offering density from 3 to 3.5 points per cm². Resampling also allowed for a reduction of the horizontal error to 0 as cells have been aligned to equal 1 cm² grid. Pictures of the point clouds from each period in RGB colors can be found in the supplementary materials for this study (Appendixes 2 and 3). A vertical error has been estimated on measurements of markers height made in the field and compared to the height received from the point clouds. In order to decrease this error source, internal closest point (ICP) algorithm was applied by registering each of the following point clouds to its variant from the previous scanning. A mentioned algorithm was performed by the "Fine registration" tool available in CloudCompare. The collective root mean square error (RMSE) of each clouds volume measurement was in the range of 0.0069 m to 0.0089 m resulting from vertical error. For comparison between each period, digital elevation model of difference (DoD) method was used.

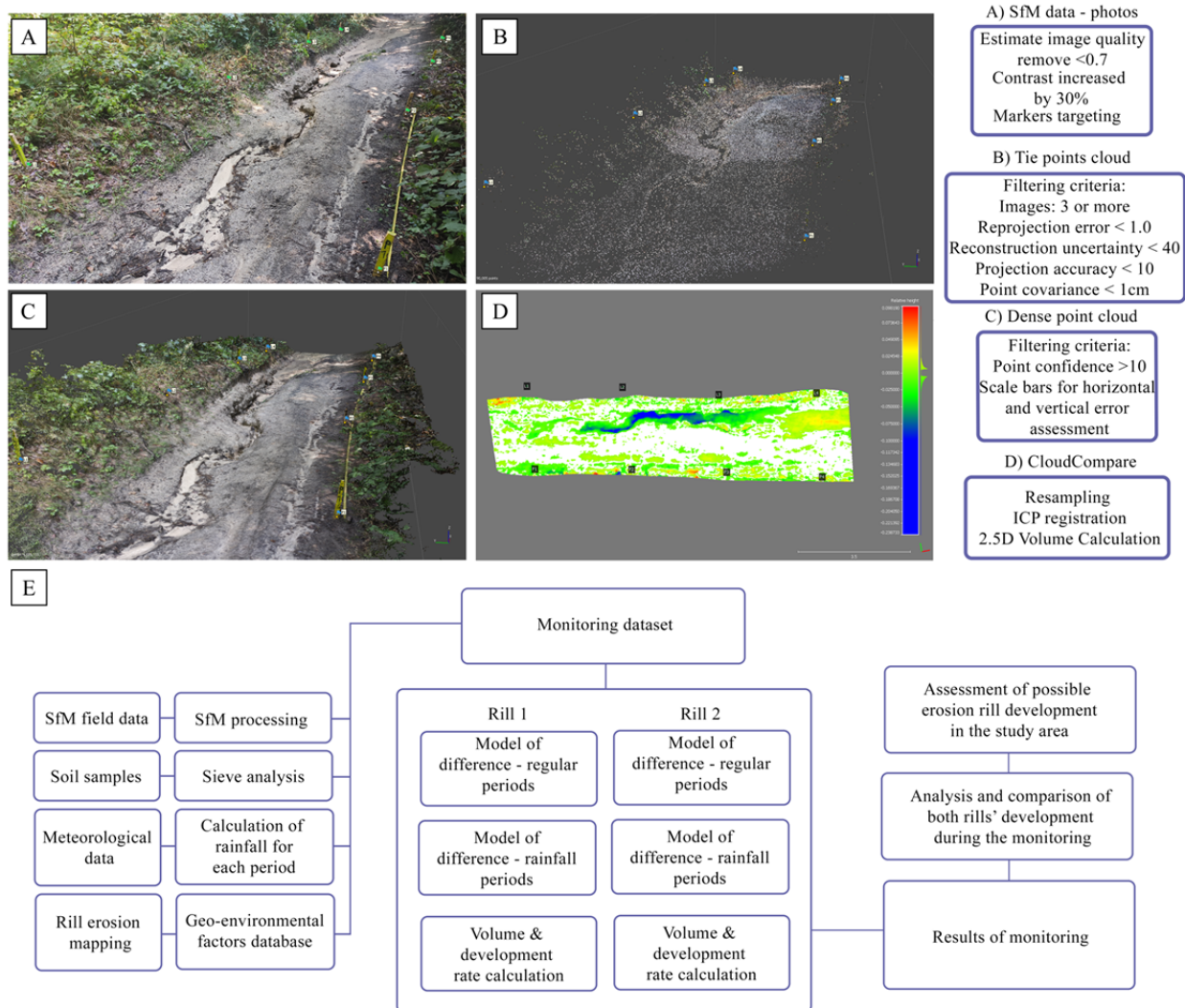Volume computation was performed by "2.5D

Fig. 3 Image processing procedure used to generate SfM point clouds with Agisoft Metashape 1.6 examples from the first testing plot, A – SfM photography; B – Camera alignment process; C – Dense point cloud; D – DoD calculation ; E – flowchart of research procedure.

volume calculator" tool in CloudCompare, which calculates volume based on the equation:

$$V_{\text{Rill}} = \sum_{n=1}^{k} (b^2 \times D_n)$$

where: V_{Rill} is Rill volume balance (m³); k is the maximum amount of cells in comparison; n is number of cell; b is the width of cell (m); D_n is the relative height difference between cells (m);

Computed volume was then multiplied by the soil density, available from laboratory analysis performed on collected soil samples from each rill. Meteorological data were obtained from the Institute of Meteorology and Water Management (IMWM) from a meteorological station 6 km from the monitored rills. Meteorological data contained the

total depth of rainfall for each period, length, and a number of rainfall events. Thus, the mean intensity has been calculated and a number of rainfall events with intensity larger than the 90th percentile of their intensity (2.7 mm/h) and longer than 0.5 hours have been counted (Table 2).

4   Results

4.1 Geometric changes analysis

During the monitoring period, both erosion rills showed soil erosion and sediment deposition, however, each of them developed differently (Fig. 4). With a newer rill (first rill) becoming larger, its

Table 2 Meteorological data for each monitored period. Number in brackets represent additional value (see table note).

Period	Length (days)		Total depth of rainfall (mm)		Number of days with rainfall >5 mm (days)		Mean intensity of >5 mm rainfall events (mm/h)	
Rill number	Rill 1	Rill 2	Rill 1	Rill 2	Rill 1	Rill 2	Rill 1	Rill 2
Spring - summer 2020	101	82	263 (87.9)[*]	237.6 (87.9)[*]	15 (6)[**]	13 (6)[**]	1.11 (7.51)[***]	1.15 (7.26)[***]
Storm event 2020	18	No data	17.9 (12.6)[*]	No data	2 (1)[**]	No data	3.44 (3.15)[***]	No data
Summer - autumn 2020	70	92	166.1 (43.4)[*]	176.4 (56)[*]	11 (3)[**]	11 (4)[**]	0.66 (8.18)[***]	0.64 (6.02)[***]
Winter 2021	167	168	170.6 (0)[*]	149.8 (0)[*]	13 (0)[**]	10 (0)[**]	0.42 (0)[***]	0.44 (0)[***]
Spring - summer 2020	93	112	194.2 (76.7)[*]	231.2 (82)[*]	17 (5)[**]	20 (6)[**]	1.12 (4.85)[***]	0.91 (5.06)[***]
Storm event 2021	45	35	201 (90.1)[*]	195 (90.1)[*]	10 (4)[**]	10 (4)[**]	1.36 (3.06)[***]	1.41 (3.06)[***]
Summer - autumn 2021	56	58	43 (0)[*]	43 (0)[*]	3 (0)[**]	3 (0)[**]	0.46 (0)[***]	0.46 (0)[***]

Note: [*] Total depth of rainfall above 90th percentile; [**] Number of days in which total depth of rainfall was above 90th percentile and longer than 0.5 h; [***] Mean intensity of rainfall events above 90th percentile and longer than 0.5 h.

volumetric development rate began to exceed the rate noted for the older more developed rill (second rill). Over time, the first rill began to develop by connecting two shallow recesses in the trail surface, after the intensive rainfall events, during the spring and summer seasons in 2020. Surface runoff created a cut that open a way for the erosion of soil particles from the deeper layers, effectively allowing for quicker development. In 2021 the rate of the volumetric development stabilized, with the first erosion rill growing in depth and size. At the beginning of monitoring the second rill has already been established, with multiple erosive forms present within the rill such as plunge pools. Three of them have been developing in size, becoming the deepest part of the erosion rill. By the end, their sizes increased, while material eroded in the process of their development often has been deposited in at their bottom. Periods with the largest areal development rate were spring - summer 2020 for the first rill (+1.7 m²) and winter 2021 for the second rill (+0.2 m²). During each SfM scanning period, both rills have had their areal development rate positive with the first rill on average 0.45 m² per scanning period while 0.1 m² on average for the second rill. The first erosion rill, starting from its developing stage was prone to area expansion as well as an increase in depth for the entire two years period. Second rill developed in size mostly next to the plunge pools which existence was an effect of surface runoff. During monitored storm events maximum incision of the first rill increased from 4 to 9 cm. While the second rill has had its sharp edges detached by the headward erosion and deposited in the plunge pools bottom effectively decreasing their depth by 6 cm. The entire development period resulted in an increase in each rill's volume. The first erosion rill increased its volume by 12% (from 4.242 m³ at the start to 4.768 m³ at the end) while for the second erosion rill this increase was equal to 9% (from 5.742 m³ at the start to 6.261 m³ at the end). Monitored storm events has been responsible for 0.11 m³ (in 2020) and 0.157 m³ (in 2021) volume increase for first rill and 0.236 m³ (in 2021) for second rill (Table 3).

4.2 Soil loss and sediment deposition analysis

The mass of eroded soil and deposited sediment balance was negative for every monitoring period with the exception of the summer-autumn 2021 period, where the balance was positive. This can be explained by the low depth of rainfall in this period (all of the days have had rainfall intensity below 90th percentile), in this period both rills recorded the smallest total soil loss. The erosion to deposition ratio for this period was below 1 for both of the studied erosion rills. Median soil erosion per rainy day (depth above 5 mm) in each given period is equal to 40.6 kg or 11.49 Mg/ha while a median of the deposited sediment is 22.45 kg or 6.35 Mg/ha. Spring - summer 2020 period has had its soil loss and sediment deposition larger than median values for both monitored erosion rills, this was an effect of larger
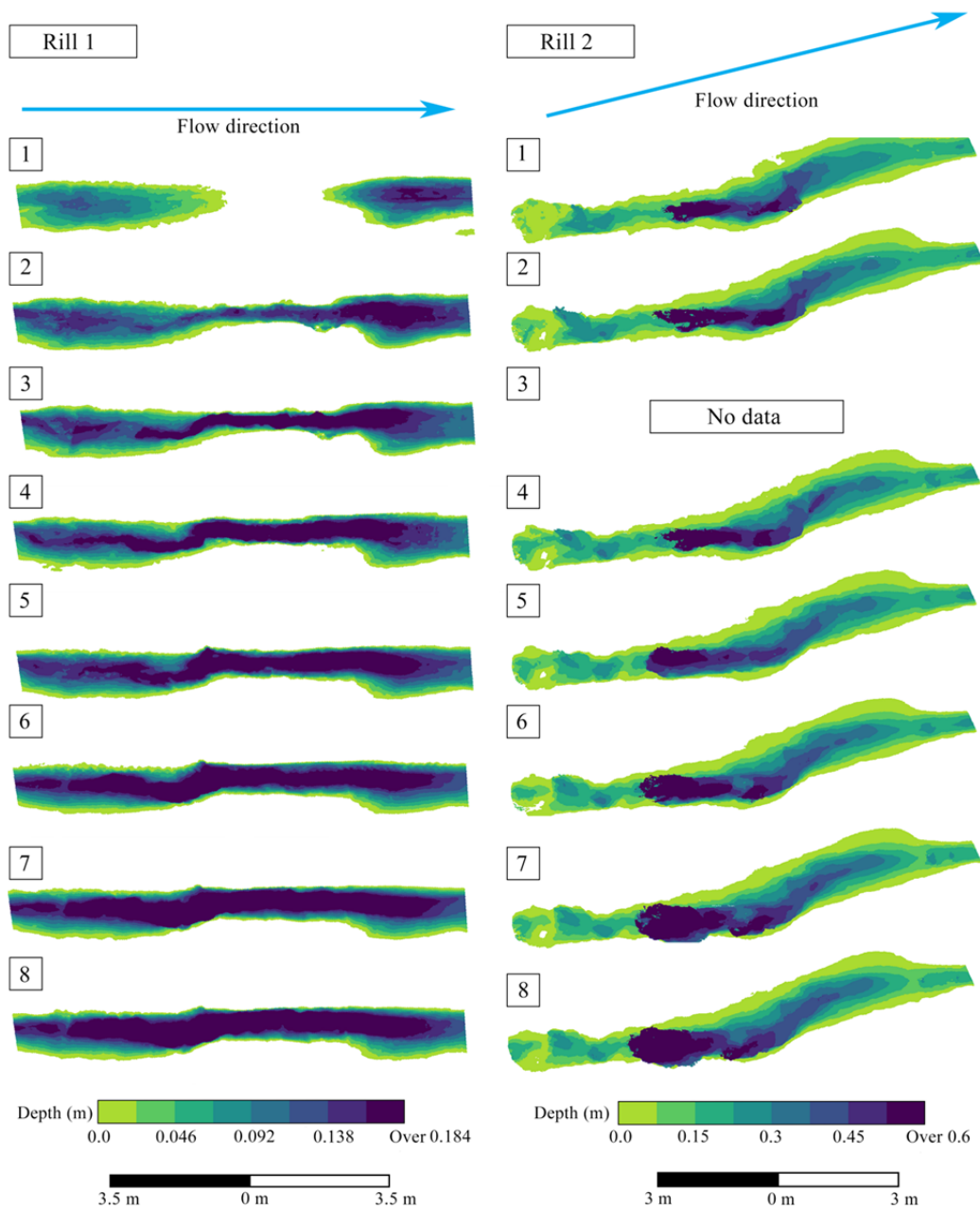
Fig. 4 Development of first and second erosion rill recorded by each SfM scanning. (1-2 represents spring to summer period in 2020; 2-3 represents storm event in 2020; 3-4 represents summer to autumn period in 2020; 4-5 represents winter period in 2021; 5-6 represents spring to summer period in 2020; 6-7 represents storm event in 2021; 7-8 represents summer to autumn period in 2021).

than usual precipitation for this period. Monitored storm events caused major changes to the erosion rills. As shorter summer storms with the length of 4 hours had over 4 times larger erosion (180.42 kg or 51.08 Mg/ha) and deposition (74.18 kg or 21 Mg/ha) than reported median values. The longer storm event (18 hours) have had over 30% larger erosion than the median value (54.6 kg or 15.45 Mg/ha) while deposition was lower than the median value (19.46 kg

or 5.5 Mg/ha). This disproportion is especially visible in the first erosion rill where the deposition was lowest during the longer storm event. The erosion to deposition ratio for this period was equal to 4.3 to 1 (Table 4). During the standard scanning periods, sediment was deposited in the nearest area below the rill, or in the case of the second rill inside of it. Most of the precipitation events were not intensive enough to generate surface runoff and carry sand

Table 3 Morphometric changes of each erosion rill during the monitoring period. Number in brackets represent additional value (see table note).

Period	Area (m²)		Maximum depth (m)		Volume (m³)	
	Rill 1	Rill 2	Rill 1	Rill 2	Rill 1	Rill 2
Spring - summer 2020	10.40 (+1.77)[*]	10.83 (+0.14)[*]	0.43 (-0.05)[*]	1.18 (+0.11)[*]	4.242 (+0.212)[*]	5.742 (+0.22)[*]
Storm event 2020	10.47 (+0.07)[*]	No data	0.52 (+0.09)[*]	No data	4.350 (+0.11)[*]	No data
Summer - autumn 2020	10.91 (+0.44)[*]	10.89 (+0.06)[*]	0.51 (-0.01)[*]	1.23 (+0.05)[*]	4.467 (+0.117)[*]	5.762 (+0.02)[*]
Winter 2021	11.12 (+0.21)[*]	11.09 (+0.20)[*]	0.47 (-0.04)[*]	0.98 (-0.25)[*]	4.521 (+0.054)[*]	5.757 (-0.005)[*]
Spring - summer 2020	11.43 (+0.31)[*]	11.12 (+0.03)[*]	0.51 (+0.04)[*]	1.3 (+0.32)[*]	4.614 (+0.093)[*]	6.032 (+0.275)[*]
Storm event 2021	11.57 (+0.34)[*]	11.25 (+0.13)[*]	0.56 (+0.04)[*]	1.24 (-0.06)[*]	4.771 (+0.157)[*]	6.268 (+0.236)[*]
Summer - autumn 2021	11.59 (+0.02)[*]	11.29 (+0.04)[*]	0.53 (-0.03)[*]	1.21 (-0.03)[*]	4.768 (-0.003)[*]	6.261 (-0.007)[*]

Note: [*] Increase or decrease of rill size in a given period.

Table 4 Erosion, deposition and mass balance during each monitoring period. Number in brackets represent additional value (see table note).

Period	Added mass (kg)		Removed mass (kg)		Mass balance (kg)		Erosion to deposition Ratio	
	Rill 1	Rill 2	Rill 1	Rill 2	Rill 1	Rill 2	Rill 1	Rill 2
Spring – summer 2020	278.41 (18.56)[*]	291.91 (22.45)[*]	723.51 (48.23)[*]	569.31 (43.79)[*]	-445.10	-277.40	2.60	1.950
Storm event 2020	148.37 (74.18)[*]	No data	360.84 (180.42)[*]	No data	-212.47	No data	2.43	No data
Summer – autumn 2020	203.32 (18.48)[*]	367.7 (33.42)[*]	446.93 (40.63)[*]	411.26 (37.39)[*]	-243.61	-43.55	2.20	1.118
Winter 2021	164.85 (12.68)[*]	553.18 (55.31)[*]	335.20 (25.78)[*]	499.96 (50.0)[*]	-170.35	53.22	2.03	0.904
Spring – summer 2020	174.01 (10.23)[*]	261.27 (13.06)[*]	324.21 (19.07)[*]	651.56 (32.58)[*]	-150.20	-390.29	1.86	2.494
Storm event 2021	86.09 (8.60)[*]	303.20 (30.32)[*]	370.00 (37.0)[*]	722.52 (72.25)[*]	-283.91	-419.32	4.30	2.383
Summer – autumn 2021	163.02 (54.33)[*]	374.16 (124.72)[*]	106.24 (35.41)[*]	356.42 (118.81)[*]	56.78	17.74	0.65	0.953

Note: [*] Added or removed mass per one day with the depth of rainfall exceeding 5 mm.

particles. During the summer period where humidity was lower and the intensity of rain larger, discharge of water was large enough to carry soil particles to the nearest streams which is why deposition values are much smaller during storm events. Recorded soil loss per year from autumn 2020 to autumn 2021 was negative and equal to 547.67 kg for the first rill and 738.65 kg for the second erosion rill, while total erosion to deposition balance for the entire monitoring period was negative and equal to: 1448.84 kg or 410 Mg/ha for the first rill and 1059.5 kg or 300 Mg/ha for the second erosion rill.

5 Discussion

5.1 SfM performance

The SfM technique and DoD method allowed for a very precise comparison of the data, which was gathered during the span of the research. The root mean square error achieved in this study was either very similar or better to the RMSE values reported in other studies (Vinci et al. 2017; Torresani et al. 2019; Fernández et al. 2020). As studied erosion rills are small and not covered by the vegetation those sources of uncertainty have been avoided, resulting in better comparison. Following the example from previous research, the horizontal error has been mitigated by the procedure of resampling to 1 cm resolution leaving vertical error as a main source of error. Yang et al. (2021) achieved even better RMSE which was

from 0.0017 to 0.003 m, compared to this study (0.0069 to 0.0089 m). However, the main difference between the circumstances of both researches was that in the former, SfM scanning was performed in laboratory conditions with fixed camera positions, rather than in the field with a smartphone camera. The performance of the SfM technique in the field was satisfying and it allowed for the realization of the goal of the research in a non-invasive way, which did not require installation of devices in the field with an exception of small wooden plugs. It was done without the use of any expensive devices, such as a terrestrial laser scanner (TLS). As mentioned in studies that compared two techniques, SfM can have benefits over TLS (Nouwakpo et al. 2015; Vinci et al. 2017). The main advantage of SfM found in this research is the mobility of the smartphone camera in capturing the deepest parts of the erosion form and its details, such as plunge pools and undercut rills edges. It is also worth noting that the time spent in the field on singular SfM scans was much shorter (from 1 to 2 hours) than that in similar studies conducted with the use of geodesic methods (from 8 to 15 hours) (Tomczyk 2010). However, the time required for the post-processing of the pictures into point clouds, took an additional 6 to 10 hours per SfM scan, which is also heavily dependent on an available graphic processor unit (GPU) used for dense cloud rendering. Another thing to consider is a deformation of the point cloud at its borders where the overlap of pictures is below 60%. This issue has been resolved by having a larger scan of an area (from 27 m² to 43 m²), where studied erosion rills ware at its center. Additional areas with larger uncertainty have been removed leaving only the structure of the rill for the measurements.

5.2 Major factors in rill erosion

The monitored erosion rills development periods recorded by the SfM technique represents examples, how can erosion rill evolution rate vary during different seasons and their sum of rainfall. One such factor that has an impact on overall development is a slope and landform gradient. Berger et al. (2010) have compared various rainfall scenarios under different landform gradients (5.71°, 11.31°, and 16.70°) in order to define their role on erosion rate. Their results show a proportion of maximum rill depth for 5.71° (33 mm) and 16.70° (88 mm) to be 0.37 to 1 which is similar to

observed in this study. The first rill with a slope of 8° and a maximum depth of 53 cm, while the second erosion rill with a slope of 15.6° and a maximum depth of 121 cm, shows a proportion of 0.43 to 1. At the same time, the proportion rate of sediment yield for both example were 0.68 to 1 (ratio of 5.71° to 16.70°) with larger erosion for the former studies while the same proportion was 0.83 to 1 (ratio of 8° to 15.6°) for this study. Aside from the gradient, a chance for the erosion rill occurrence and its rate of development is increased by the position and orientation towards the slope direction. With a smaller angle between the rill axis of length and slope direction, surface runoff has an easier way to drain the road's surface, creating erosion rills as a result (Leung and Marion 1996; Marion 2008). This relation confirms the state of both erosion rills as the first one with better orientation (37° angle), position and smaller runoff contribution area did not develop plunge pools, which are the main factor in the growth of the second erosion rill, which has a poorer orientation (near 0° angle towards slope direction), position and larger runoff contribution area (Table 1). Another factor that possibly impacted the erosion rill development was the use of the trail by pedestrians, bikes and vehicles as it is still located at the main road. At the beginning of the monitoring period, the second erosion rill has already been omitted by the users of the route, which resulted in the creation of a new path. This difference is visible in overall soil loss for the entire monitoring period which was 37% larger for the first erosion rill. Despite the better position, orientation and lower landform grade, first erosion rill has had a larger total soil loss than the second rill which has far better conditions for erosion. Froehlich (1980) noted the destructive effect of wheels and vehicle braking systems on unpaved roads, while the negative impact of use-related factors has also been confirmed in other studies (Ballantyne and Pickering 2015; Salesa and Cerdà 2020). Asides from mentioned factors both monitored erosion rills were similar in size, received a similar amount of rainfall, and have had the same forested landcover. Overall soil properties were also similar in both rills, with the same relation noted by Phillips and Marion (2020), who has found a smaller amount of fine sediment within trail systems that were exposed to the overland flow of water in comparison to the areas unaffected by surface runoff. As the presented comparison shows, factors such as slope, road segment length, and runoff

contribution area have a noticeable impact on the rills development process. This confirms the findings of similar research conducted by Cao et al. (2021) with the use of TLS on unpaved roads.

5.3 Study implication

Recorded observations during the monitoring, as well as erosion rates for a specific set of conditions, allowed for the identification of the rills' development rate. Therefore, such information can be a foundation for a machine learning modeling application where it is necessary to obtain training materials in order to achieve the high accuracy of the models and predict possible development scenarios, as it was done in recently conducted research with the use of machine learning techniques (Wang et al. 2021; Chen et al. 2022). With every SfM scan performed in the field, both rills have had increased in size. Increases in the area and depth of each rill indicate the future development of a permanent slit and even a gully, as stated by Lach (1984). Fidelus-Orzechowska et al. (2021) studied the development rate of degradation zones on hiking trails in Tatra National Park and found an areal increase per year from 0.04 to 0.16 m²/m/year. For comparison, the areal development rate of erosion rills found in this study has been in a similar range from 0.047 to 0.132 m²/m/year. The volume of the displaced material was greater than that reported in another similar study (Tomczyk 2010) (0.083 m³ to 0.11 – 0.236 m³ in this study). Upon closer inspection of the test field chosen for that study, not only was it in a different developmental stage (a much thinner and shallower rill) but also, the testing plot has been smaller in size compared to this study. Another example of a rainstorm event and its effect on unpaved roads has been described in studies conducted in China (Zhang et al. 2019). Their volumetric results showed much greater (up to 20 times) damage to the road than that observed in this research. However, this greater damage was the effect of catastrophic storms and floods that occurred in just two days with over 250 mm of rainfall, which was approximately 20 times larger than that observed in this study in 2020. With the number of rills counted during preliminary field investigation (92 rills per 12 km out of which 20 is deeper than 30 cm), assumed number of regular erosion rills with a potential to develop further within 62.5 km of the trails in Posłowickie mountain range may even be 479 out of

which over 100 already developed to or past the stage of the monitored rills. Thus the total sediment yield from the southern part of Kielce, originating only from the rills development, may be in the range of 54.7 – 73.9 Mg/year (0.88 – 1.18 Mg/km/year) with a potential to grow up to 262.3 – 353.8 Mg/year (4.19 – 5.66 Mg/km/year) once all of the potential rills fully develop. Zhang et al. (2019) also found a similar amount of rills while studying unpaved road network in China's Loess Plateau (85 rills per 10.5 Km to 92 rills per 12 Km in this study). This indicates that the unpaved roads of the Holy Cross Mountains are very susceptible to rill erosion. As the results show, from 52% to 56% of the soil loss from the monitored rills in 2021 is a result of storm events during summer. Kielce city is an area that is already known for significant sedimentation. Ciupa (2009) calculated alluvial transport of the city's main river Silnica in which transport of dissolved solids, suspended sediment and riverbed load combined have been over 7000 Mg/year. Wałek (2019) found an increase in sediment transportation in urban sub-catchment, during summer periods after the intensive rainfall events. Therefore, adding new potential sources of sedimentation in the form of hundreds of unpaved road gullies should be avoided.

6 Conclusion

With a dynamic climate change, extreme events such as droughts and intensive rainfalls might occur more often than in the past affecting the temperate zone. At the same time, increasing human impact on the hiking trails represents a growing problem of management and land conservation. In Posłowickie mountain range, potential rill erosion can grow up to 5 times in comparison to the current, while hundreds of developing erosion forms can develop into permanent road gullies, eventually transporting sediment to the Silnica river valley where Kielce city is located. The development of the monitored erosion rills was dependent on multiple factors such as road gradient, the shape of the rill, season and its depth of rainfall. With the larger road gradient, rills are often created near the series of plunge polls that connect into the singular structure, while with the smaller gradient, surface runoff cuts through the surface. Recorded rills have presented that the process of development can be very fast, which can last from less

than 3 years up to 10 years before reaching a developed stage while at the same time, surface runoff caused by the intensive rainfall event, can speed this process to just a few days, as presented in the case of the first rill. This gives little time to react in order to perform hiking trail maintenance and shows, that a detection system of potential rills should be applied to prevent their development. In order to build up such system, scientists have attempted modeling based on statistical methods such as regression trees, logistic regression, and random forest, integrated into geographical information systems (GIS). Usage of such systems by the land managers could result in decisions that prevent erosion and a need for, often costly surface reconstructions procedures.

References

Angulo-Martinez M, Begueria S, Navas A, et al. (2012) Splash erosion under natural rainfall on three soil types in NE Spain. Geomorphology 175: 38-44.
https://doi.org/10.1016/j.geomorph.2012.06.016
Arnáez J, Larrea V, Ortigosa L (2004) Surface runoff and soil erosion on unpaved forest roads from rainfall simulation tests in northeastern Spain. Catena 57(1): 1-14.
https://doi.org/10.1016/j.catena.2003.09.002
Ballantyne M, Pickering CM (2015) The impacts of trail infrastructure on vegetation and soils: Current literature and future directions. J Environ Manag 164: 53-64.
https://doi.org/10.1016/j.jenvman.2015.08.032
Berger C, Schulze M, Rieke-Zapp D, et al. (2010) Rill development and soil erosion: a laboratory study of slope and rainfall intensity. Earth Surf Process Landf 35(12): 1456-1467.
https://doi.org/10.1002/esp.1989
Beullens J, de Velde DV, Nyssen J (2014) Impact of slope aspect on hydrological rainfall and on the magnitude of rill erosion in Belgium and northern France. Catena 114: 129-139.
https://doi.org/10.1016/j.catena.2013.10.016
Bouchnak H, Felfoul MS, Boussema MR, et al. (2009) Slope and rainfall effects on the volume of sediment yield by gully erosion in the Souar lithologic formation (Tunisia). Catena 78(2): 170-177. https://doi.org/10.1016/j.catena.2009.04.003
Cao L, Wang Y, Liu C (2021) Study of unpaved road surface erosion based on terrestrial laser scanning Catena 199: 105091. https://doi.org/10.1016/j.catena.2020.105091
Ciupa T (2009) The impact of land use runoff and fluvial transport in small river catchments: Based on the Sufraganiec and Silnica Rivers (Kielce, Poland). Jan Kochanowski University: Kielce, Poland. (in Polish)
Ciupa T, Suligowski R (2020) Impact of the city on the rapid increase in the runoff and transport of suspended and dissolved solids during rainfall—The example of the Silnica River (Kielce, Poland). Water 12: 2693.
https://doi.org/10.3390/w12102693
Chaplot V, Brown J, Dlamini P, et al. (2011) Rainfall simulation to identify the storm-scale mechanisms of gully bank retreat. Agr Water Manag 98(11): 1704-1710.
https://doi.org/10.1016/j.agwat.2010.05.016
Chen Ch, Zhang Q, Kashani MH, et al. (2022) Forecast of rainfall distribution based on fixed sliding window long short-term memory. Eng Appl Comput Fluid Mech 16(1): 248-261.
https://doi.org/10.1080/19942060.2021.2009374
Cole DN (1991) Changes on trails in the Selway-Bitterroot Wilderness, Montana, 1978-89. Res. Pap. INT-RP-450. Ogden, UT: U.S. Department of Agriculture, Forest Service,

Intermountain Research Station. 5 p.
Comino JR, Brings C, Lassu T, et al. (2015) Rainfall and human activity impacts on soil losses and rill erosion in vineyards (Ruwer Valley, Germany). Solid Earth 6(3): 823-837.
https://doi.org/10.5194/se-6-823-2015
Fang H, Sun L, Tang Z (2014) Effects of rainfall and slope on runoff, soil erosion and rill development: an experimental study using two loess soils. Hydrol Process 29(11): 2649-2658.
https://doi.org/10.1002/hyp.10392
Fernández T, Gómez-Lopez JM, Pérez-García JL, et al. (2020) Analysis of gully erosion in a catchment area in olive groves using uas photogrammetry techniques. Int Arch Photogramm, Remote Sens Spat Inf Sci 43: 1057-1064.
https://doi.org/10.5194/isprs-archives-XLIII-B2-2020-1057-2020
Fidelus-Orzechowska J, Gorczyca E, Bukowski M, et al. (2021) Degradation of a protected mountain area by tourist traffic: case study of the Tatra National Park, Poland. J Mt Sci 18: 2503-2519. https://doi.org/10.1007/s11629-020-6611-4
Filonowicz P (1973) Explanations to the Detailed Geological Map of Poland in the scale of 1: 50,000 (Kielce sheet). Polish Geological Institute (in Polish).
Froehlich W, Walling DE (1997) The role of unmetalled roads as a sediment source in the fluvial systems of the Polish Flysch Carpathians. Human impact on erosion and sedimentation (Proceedings of an international symposium of the Fifth Scientific Assembly of the International Association of Hydrological Sciences, Rabat, Morocco, 23 April to 3 May 1997. Wallingford: IAHS Press: 159-168.
Eagleston H, Marion JL (2020) Application of airborne LiDAR and GIS in modeling trail erosion along the Appalachian Trail in New Hampshire, USA. Landsc Urban Plan 198: 103765.
https://doi.org/10.1016/j.landurbplan.2020.103765
Govers G, Giménez R, Oost KV (2007) Rill erosion: Exploring the relationship between experiments, modelling and field observations. Earth Sci Rev 84(3-4): 87-102.
https://doi.org/10.1016/j.earscirev.2007.06.001
He JJ, Sun LY, Gong HL, et al. (2017) Laboratory studies on the influence of rainfall pattern on rill erosion and its runoff and sediment characteristics. Land Degrad Dev 28(5): 1615-1625.
https://doi.org/10.1002/ldr.2691
Kiani-Harchegani M, Sadeghi SH, Asadi H (2018) Comparing grain size distribution of sediment and original soil under raindrop detachment and raindrop-induced and flow transport mechanism. Hydrol Sci J 63(2): 312-323.
https://doi.org/10.1080/02626667.2017.1414218
Kopyść PT (2020) The use of aerial LiDAR and Structure from

Motion (SfM) Photogrammetry data in analyzing microtopographic changes on hiking trails on the example of Kielce (Poland). Carpathian J Earth Environ Sci 15(2): 461-470. https://doi.org/10.26471/cjees/2020/015/145

Lach J (1984) Geomorphological effects of agricultural anthropopressure in selected parts of the Carpathians and their foothills. Monographic works of the WSP im. KEN in Cracow, No. LXVI. Scientific Publisher WSP: 120 (in Polish).

Leung YF, Marion JL (1996) Trail degradation as influenced by environmental factors: A state of the knowledge review. J Soil Water Conserv 51: 130-136.

Marion JL (2008) Trail and campsite monitoring protocols: Zion National Park. U.S. Geological Survey, Technical Report.

Martnez-Casasnovas JA, Ramos MC, Ribes-Dasi M (2002) Soil erosion caused by extreme rainfall events: mapping and quantification in agricultural plots from very detailed digital elevation models. Geoderma 105(1-2): 125-140. https://doi.org/10.1016/s0016-7061(01)00096-9

Meadema F, Marion JL, Arredondoa J, et al. (2020) The influence of layout on Appalachian Trail soil loss, widening, and muddiness: Implications for sustainable trail design and management. J Environ Manag 257(2): 109986. https://doi.org/10.1016/j.jenvman.2019.109986

Michalczyk Z, Chmiel S, Głowacki S, et al. (2012) Surface runoff in the urbanized catchment of Głęboka street in Lublin in the summer season of 2011. Teka 9: 107-115.

Mityk J (1993) Recreational areas in the vicinity of Kielce. Kielce: Wyższa Szkoła Pedagogiczna im. Jana Kochanowskiego (in Polish)

Nourani N, Alali N, Samadianfard S, et al. (2022) Comparison of machine learning techniques for predicting porosity of chalk. J Pet Sci Eng 209: 109853. https://doi.org/10.1016/j.petrol.2021.109853

Nouwakpo SK, Weltz MA, McGwire K (2015) Assessing the performance of structure-from-motion photogrammetry and terrestrial LiDAR for reconstructing soil surface microtopography of naturally vegetated plots. Earth Surf Process 41: 308-322. https://doi.org/10.1002/esp.3787

Ou X, Hu Y, Li X, et al. (2021), Advancements and challenges in rill formation, morphology, measurement and modeling. Catena 196: 104932. https://doi.org/10.1016/j.catena.2020.104932

Phillips JD, Marion DA, Kilcoyne KG (2020) Fine sediment storage in an eroding forest trail system. Phys Geogr 42(1): 50-72. https://doi.org/10.1080/02723646.2020.1743613

Sadeghian N, Vaezi AR, Majnooniheris A, et al. (2021) Soil physical degradation and rill detachment by raindrop impact in semi-arid region. Catena 207: 105603. https://doi.org/10.1016/j.catena.2021.105603

Salesa D, Cerdà A (2020) Soil erosion on mountain trails as a consequence of recreational activities. A comprehensive review of the scientific literature. J Environ Man 271: 13. https://doi.org/10.1016/j.jenvman.2020.110990

Salesa D, Minervino Amodio A, Rosskopf CM, et al. (2020) Three topographical approaches to survey soil erosion on a mountain trail affected by a forest fire. Barranc de la Manesa, Llutxent, Eastern Iberian Peninsula. J Environ Man 264(5): 110491. https://doi.org/10.1016/j.jenvman.2020.110491

Sahani N, Ghosh T (2021) GIS-based spatial prediction of recreational trail susceptibility in protected area of Sikkim Himalaya using logistic regression, decision tree and random forest model. Ecol Inform 64: 101352. https://doi.org/10.1016/j.ecoinf.2021.101352

Szeląg B, Suligowski R, Studziński J, et al. (2020) Application of logistic regression to simulate the influence of rainfall genesis on storm overflow operations: a probabilistic approach. Hydrol Earth Syst Sci 24: 595-614. https://doi.org/10.5194/hess-24-595-2020

Shen H, Zheng F, Wen L, et al. (2015) An experimental study of rill erosion and morphology. Geomorphology 231: 193-201. https://doi.org/10.1016/j.geomorph.2014.11.029

Shen HO, Wen LL, He YF, et al. (2018) Rainfall and inflow effects on soil erosion for hillslopes dominated by sheet erosion or rill erosion in the Chinese Mollisol region. J Mt Sci 15(10): 2182-2191. https://doi.org/10.1007/s11629-018-5056-5

Shen HO, Zheng FL, Wang L, et al. (2019) Effects of rainfall intensity and topography on rill development and rill characteristics on loessial hillslopes in China. J Mt Sci 16(10): 2299-2307. https://doi.org/10.1007/s11629-019-5444-5

Starkel L (2011) Temporal and spatial complexity of extreme rainfalls – their geomorphological effects and ways of counteract them. LA. Landf Anal 15: 65-80 (in Polish).

Strzemski M (1965) Lithological and soil-forming regions of the Kielce voivodship. Soil Sci Ann 15. Polskie Towarzystwo Gleboznawcze (in Polish).

Suligowski R (2014) Maximum rainfall depth of specified duration and probability of exceedance in Kielce, in Ciupa T, Suligowski R (eds.) Water in the city. Hydrological Commission Monographs PTG 2: 271-280. ISBN 978-83-60026-50-2 (in Polish).

Tomczyk A (2010) Digital models of microrelief and their use in study of the dynamics of changes in tourist trails surfaces. LA Landf Anal 12: 127-136 (in Polish).

Tomczyk AM, Ewertowski M (2013) Planning of recreational trails in protected areas: Application of regression tree analysis and geographic information systems. Appl Geogr 40: 129-139. https://doi.org/10.1016/j.apgeog.2013.02.004

Tomczyk A, White P, Ewertowski M (2016) Effects of extreme natural events on the provision of ecosystem services in a mountain environment: the importance of trail design in delivering system resilience and ecosystem service co-benefits. J Environ Manag 166: 156-167. https://doi.org/10.1016/j.jenvman.2015.10.016

Torresani L, Wu J, Masin R, et al. (2019) Estimating soil degradation in montane grasslands of North-eastern Italian Alps (Italy). Heliyon 5: e01825. https://doi.org/10.1016/j.heliyon.2019.e01825

Trenberth K (2011) Changes in precipitation with climate change. Clim Res 47: 123-138. https://doi.org/10.3354/cr00953

Vinci A, Todisco F, Brigante R, et al. (2017) A smartphone camera for the structure from motion reconstruction for measuring soil surface variations and soil loss due to erosion. Hydrol Res 48: 673-686. https://doi.org/10.2166/nh.2017.075

Wałek G (2019) The influence of roads on surface runoff formation in the urbanized area on the example of Silnica River catchment in Kielce. Jan Kochanowski University: Kielce, Poland. (in Polish)

Wang C, Liu B, Yang Q, et al. (2021) Unpaved road erosion after heavy storms in mountain areas of northern China. Int Soil Water Conserv Res (in press) https://doi.org/10.1016/j.iswcr.2021.04.012

Wang F, Sahana M, Pahlevanzadeh B, et al. (2021) Applying different resampling strategies in machine learning models to predict head-cut gully erosion susceptibility. Alex Eng J 60(6): 5813-5829. https://doi.org/10.1016/j.aej.2021.04.026

Wimpey JF, Marion JL (2010) The influence of use, environmental and managerial factors on the width of recreational trails. J Environ Man 91: 2028-2037. https://doi.org/10.1016/j.jenvman.2010.05.017

Woo MK, Fang G, di Cenzo PD (1997), The role of vegetation in the retardation of rill erosion. Catena 29(2): 145-159. https://doi.org/10.1016/s0341-8162(96)00052-5

Xu Q, Li WL, Ju YZ, et al. (2020) Multitemporal UAV-based photogrammetry for landslide detection and monitoring in a large area: a case study in the Heifangtai terrace in the Loess Plateau of China. J Mt Sci 17(8): 1826-1839. https://doi.org/10.1007/s11629-020-6064-9

Yang Y, Shi Y, Liang X, et al. (2021) Evaluation of structure from motion (SfM) photogrammetry on the measurement of rill and interrill erosion in a typical loess. Geomorphology 385: 107734. https://doi.org/10.1016/j.geomorph.2021.107734

Zhang Y, Zhao Y, Liu B, et al. (2019) Rill and gully erosion on unpaved roads under heavy rainfall in agricultural watersheds on China's Loess Plateau. Agric Ecosyst Environ 284: 106580. https://doi.org/10.1016/j.agee.2019.106580

Yang ZS, Liang LH(2004) Soil erosion under different land use types and zones of Jinsha River Basin in Yunnan Province, China. J Mt Sci 1(1): 46-56.